Role of Chain Length in the Formation of Frank-Kasper Phases in Diblock Copolymers

Ronald M. Lewis, III, Akash Arora, Haley K. Beech, Bongjoon Lee, Aaron P. Lindsay, Timothy P. Lodge, Kevin D. Dorfman, and Frank S. Bates

Phys. Rev. Lett. **121**, 208002 — Published 14 November 2018

DOI: 10.1103/PhysRevLett.121.208002

Role of chain length in the formation of Frank-Kasper phases in diblock copolymers

Ronald M. Lewis III,[1] Akash Arora,[1] Haley K. Beech,[1] Bongjoon Lee,[1] Aaron P. Lindsay,[1]

Timothy P. Lodge,[1,2] Kevin D. Dorfman,[1] and Frank S. Bates[1,*]

[1]*Department of Chemical Engineering and Materials Science and*

[2]*Department of Chemistry, University of Minnesota, Minneapolis, MN 55455, USA*

**To whom correspondence should be addressed:* bates001@umn.edu

Abstract:

The phase behavior of poly(styrene)-*b*-poly(1,4-butadiene) diblock copolymers with polymer block invariant degree of polymerization $\bar{N}_b \approx 800$ shows no evidence of Frank-Kasper phases, in contrast to low molar mass diblock copolymers ($\bar{N}_b < 100$) with the same conformational asymmetry. A universal self-concentration crossover parameter $\bar{N}_x \approx 400$ is identified, directly related to the crossover to entanglement dynamics in polymer melts. Mean-field behavior is recovered when $\bar{N}_b > \bar{N}_x$, while complex low symmetry phase formation is attributed to fluctuations and space-filling constraints, which dominate when $\bar{N}_b < \bar{N}_x$.

Recent discoveries involving mesoscopic particles formed by self-assembled dendrimers [1–4], surfactants [5–7], and block polymers [8–10] have revealed a variety of low-symmetry periodic and aperiodic states of order with particle dimensions ranging from several to tens of nanometers. These tetrahedrally coordinated Frank-Kasper [11,12] and quasicrystalline phases are strikingly similar to those found in many types of metals [13,14] and alloys [15], offering enticing opportunities to establish the universal principles that govern the organization of dense arrays of particles in condensed matter [16]. Block polymers are especially interesting owing to molecular simplicity and remarkable consistency between experiments and self-consistent mean-field theory (SCFT), the most powerful predictive tool in the theoretical arsenal directed at the phase behavior of block polymers. Occurrence of the Frank-Kasper σ phase in AB diblock copolymers has been associated with differences in the way each polymer block pervades space, referred to as conformational asymmetry [17,18]. However, the σ phase has been reported only in low molecular

weight diblock copolymers, and at significantly smaller conformational asymmetry than is anticipated by SCFT [17,18]. Here we show that the emergence of Frank-Kasper phases in block polymers is also influenced by chain length, expressed through the invariant degree of polymerization of a block $\bar{N}_b = Nb^6/v^2$ where N is the number of repeat units with statistical segment length b and volume v.

Establishing the universal principles that relate physical properties to N is a central goal of polymer physics. The degree of polymerization plays a dominant role in many thermodynamic and dynamic phenomena including the phase behavior of polymer blends, order and disorder in block polymers, and viscoelasticity in polymer melts and solutions. Undiluted polymer melts execute a random walk leading to a radius of gyration $R_g = b(N/6)^{1/2}$. As N increases the number of contacts between a given polymer chain and other chains in the melt increases and, concomitantly, the self-concentration $\varphi_s = V_{occupied}/V_{pervaded} \sim \bar{N}^{-0.5}$ decreases. A particularly noteworthy manifestation of this change in self-concentration with N is the dependence of polymer viscosity on chain length, $\eta \sim N^{3.4}$, which is associated with molecular entanglements in reptation theory [19]. As N is reduced, increasing polymer self-concentration squeezes out entanglements leading to a crossover to the Rouse regime $\eta \sim N^1$ near an entanglement molecular weight $M_e = N_e \rho N_{av} v$, where N_e, ρ, and N_{av} are the entanglement degree of polymerization, polymer density, and Avogadro's number, respectively [20]. Simple molecular packing arguments lead to $N_e = Av^2b^{-6}$, where A is a universal constant [21–23].

Self-concentration also impacts diblock copolymers resulting in a fluctuation-induced first-order order-disorder transition (ODT) between the lamellar (lam) and disordered (dis) states. Recent advances in modeling composition fluctuations in compositionally symmetric diblocks ($f_A = N_A/N = ½$) have extended the fluctuation-corrected RPA theory of Fredrickson and Helfand yielding $(\chi N)_{ODT} = 10.495 + 41.0\,\bar{N}^{-1/3} + 123.0\,\bar{N}^{-0.56}$, where $N = N_A + N_B$ and χ is the Flory-Huggins segment-segment interaction parameter [24,25]. Series expansions of this type are predicated on perturbations away from the mean-field case of infinite overlap ($\bar{N} \to \infty$), and should break down when the self-concentration becomes too high [25]. We speculate that this relationship

will fail at block molecular weights $\bar{N}_b < \bar{N}_x$, where $\bar{N}_x \approx N_e b^6/v^2 = A$ by analogy with the crossover from Rouse to reptation dynamics, which is governed by the same self-concentration effects that interfere with the assumptions implicit in the fluctuation theory. Based on literature data for the entanglement molecular weight, density, and b values for over two dozen polymer melts, $A = 370 \pm 87$ (95 % confidence interval, see Table S3 [26]); $\bar{N}_x \approx 400$ is consistent with the point at which the renormalized one-loop (ROL) theory fails to account for molecular simulation results [25,38,39].

Compositional asymmetry, $f_A \neq ½$, introduces interfacial curvature into the free energy competition that determines the equilibrium morphology in ordered diblock copolymers, leading to bicontinuous (double gyroid and *Fddd*), cylindrical, and spherical domain geometries. Differences in repeat unit chemistry result in differences in the volume pervaded by each block per unit contour length, which is captured by the conformational asymmetry parameter $\varepsilon = b_A^2 / b_B^2$ (defined such that $\varepsilon \geq 1$) [40]. SCFT predicts that conformational asymmetry, $\varepsilon > 1$, skews the theoretical mean-field phase portrait, f_A versus χN, and opens a window of Frank-Kasper phases at $f_A < ½$ when $\varepsilon > 2.25$ in the limit $\chi N >> (\chi N)_{ODT}$ [17]. Recently we showed that increasing ε indeed leads to the development of the σ phase in model low molecular weight diblock copolymers [18]. However, this complex, low symmetry ordered structure appears at significantly smaller values of ε than predicted by SCFT as illustrated in Fig. 1, which compares the calculated and experimental phase behavior for poly(ethylethylene)-*b*-poly(±-lactide) (EL), where $\varepsilon = 1.7$. (The experimental data from Ref. [18] have been rescaled by calculating $\chi(T)$ using published data and the recent simulation-based predictions for compositionally symmetric AB copolymers as described in the Supplemental Material [26].) Significantly, $\bar{N}_b \approx 80$ in the EL system, which is much smaller than the value of $\bar{N}_x$ estimated based on polymer melt dynamics. Two important features are revealed by Fig. 1. First, the small $\bar{N}$ elevates $(\chi N)_{ODT}$ for EL, as anticipated by fluctuation theory. Second, whereas the mean-field theory predicts only body-centered cubic (bcc) and hexagonally packed cylinder (hex) phases for monodisperse diblocks with $\varepsilon = 1.7$, the experimental map contains a wide composition window of the σ phase ($0.18 < f_{PLA} < 0.25$) between

these morphologies. (We note that increasing the dispersity of the polymer blocks also opens a window of Frank-Kasper phases in the SCFT phase portrait for values of ε < 2.25 [41].) Surprisingly, there were no reports of the σ phase for diblock copolymers prior to 2010 notwithstanding more than four decades of intensive research on numerous diblock copolymer systems, including detailed investigations into the role of composition fluctuations near the order-disorder transition temperature (T_{ODT}) in compositionally asymmetric, bcc-forming poly(styrene)-*b*-poly(isoprene) (SI) [42–44].

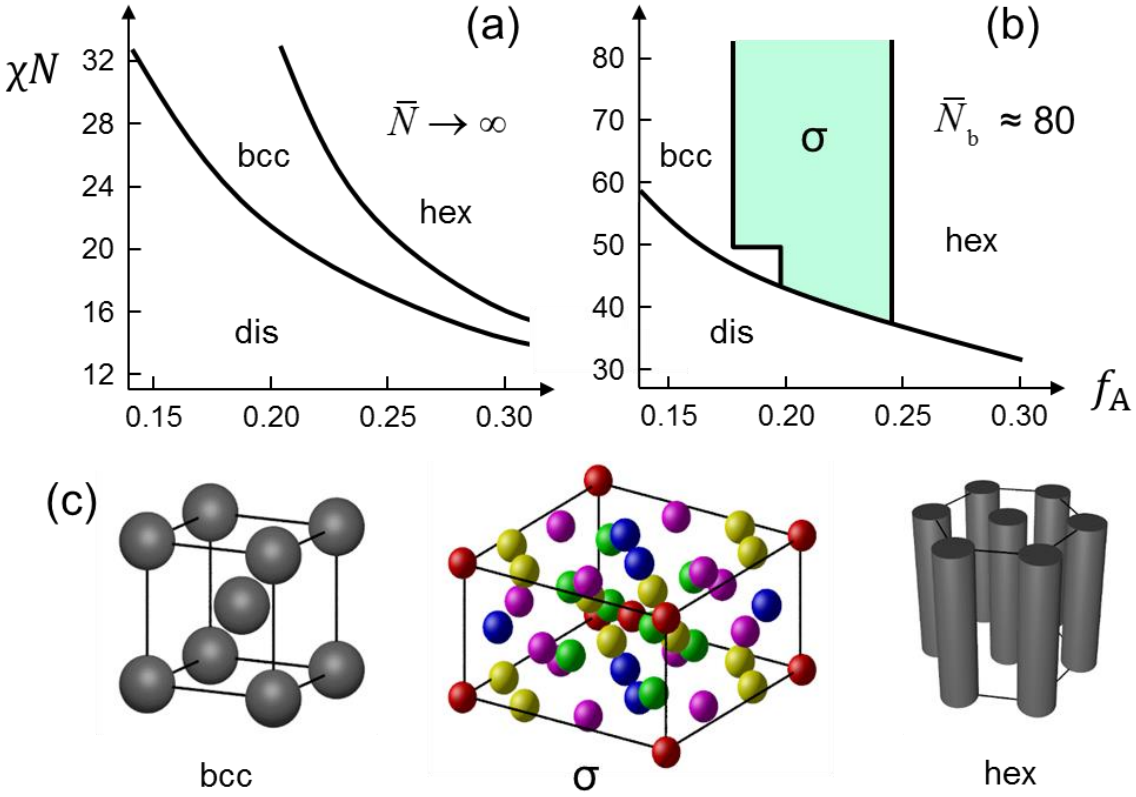

FIG 1. Phase maps based on (a) SCFT calculations and (b) experiments for the EL system reported by Schulze *et al*. where ε = 1.7 [18]. $\bar{N}_b$ refers to an average of the invariant degree of polymerization of the blocks. In contrast to theory, experiments reveal the Frank-Kasper σ phase located at compositions between the bcc and hex phases as illustrated in (c).

The goal of this paper is to establish the origins of this discrepancy between SCFT predictions and the experimentally observed phase behavior. To this end we prepared two narrow dispersity $Đ = M_w/M_n$ poly(styrene)-*b*-poly(1,4-butadiene) (SB; see Fig. 2a) diblock copolymers (SB-20: M_n

= 26.7 kDa, $Đ$ = 1.06, f_{PB} = 0.198; SB-25: M_n = 31.3 kDa, $Đ$ = 1.06, f_{PB} = 0.249; see Fig. 2a and Supplemental Material [26]). These polymers are characterized by ε = 1.7 (see Supplemental Material [26]), which within experimental error matches that of the EL system shown in Fig. 1b. By selecting polymer blocks with a smaller χ parameter than that associated with EL, we were able to increase the invariant degree of polymerization of each block by approximately an order of magnitude ($\bar{N}_b \approx 800$ based on M_n from ^{1}H NMR spectroscopy), while maintaining T_{ODT} at experimentally accessible values. Order-disorder transition temperatures were determined through dynamic mechanical thermal analysis (DMTA) by monitoring the dynamic elastic modulus G' while heating the materials at 1 ºC/min; a discontinuous drop in elasticity indicates the T_{ODT} as shown in Fig. 2d, where $T_{ODT,SB-20}$ = 153 ± 1 ºC and $T_{ODT,SB-25}$ = 226 ± 1 ºC. The two diblock copolymer compositions were chosen to access the predicted spherical bcc and cylindrical hex phases, which were confirmed using transmission electron microscopy (TEM) and small-angle x-ray scattering (SAXS) experiments. TEM images obtained from OsO_4 stained, thin (ca. 70 nm) cryo-microtomed sections of the polymers following annealing at temperatures below T_{ODT} reveal well-ordered particles and hexagonally arranged cylindrical domains for SB-20 and SB-25, as shown in Figs. 2b and 2c, respectively. SAXS powder patterns recorded at the Advanced Photon Source at Argonne National Laboratory using λ = 0.7293 Å wavelength radiation confirm bcc order in SB-20 (Fig. 3A) and hex symmetry in SB-25 (Fig. 3C), as well as T_{ODT}s that are consistent with the DMTA results. Here we note that absence of the third-order Bragg reflection at $q = \sqrt{4}q^*$ (where $q = 4\pi\sin(\theta/2)/\lambda$ and q^* is the first-order reflection) in the SAXS patterns for SB-25 (Fig. 3C) is due to a form factor extinction associated with the cylindrical morphology as shown in the Supplemental Material [26].

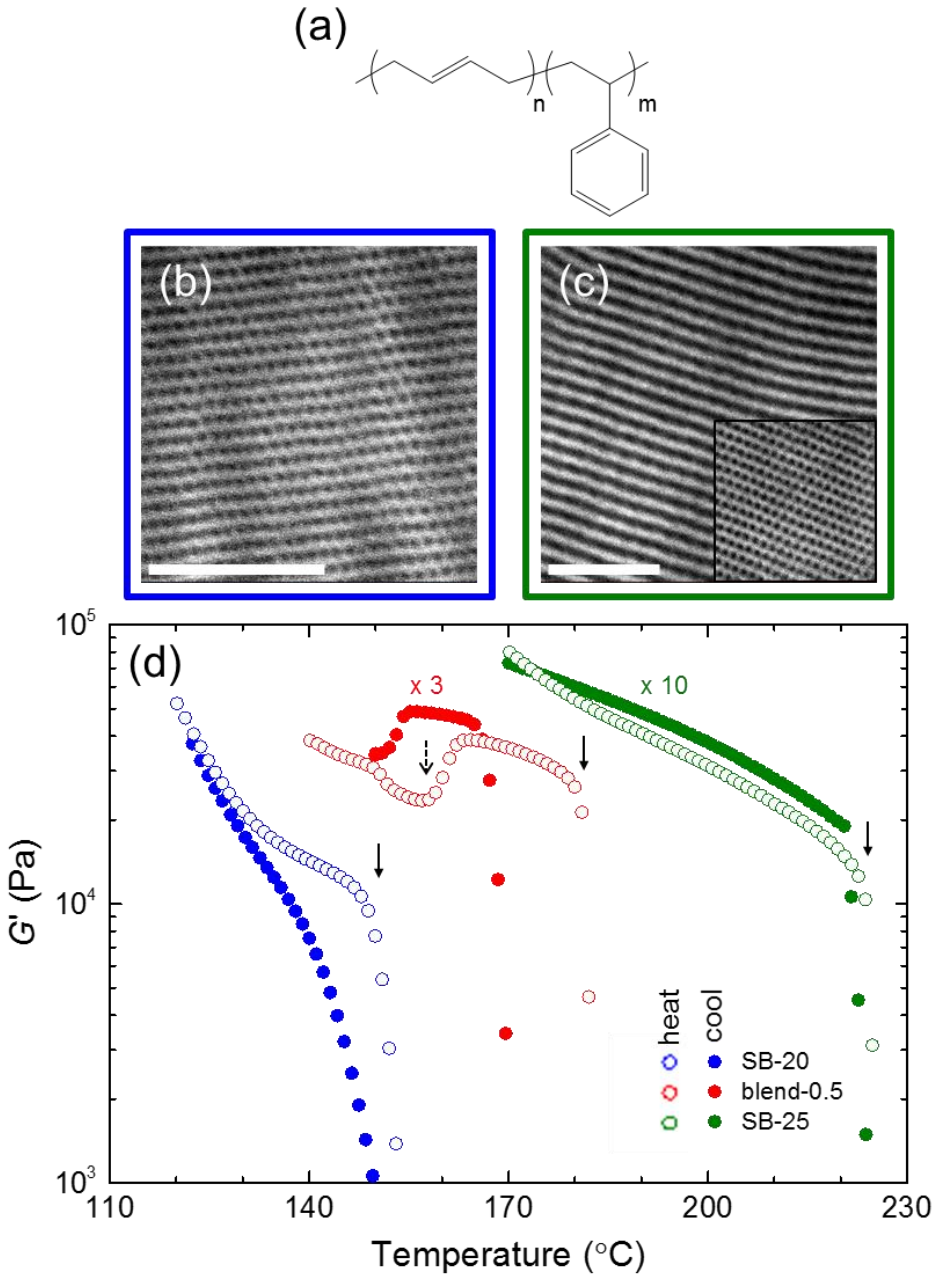

FIG 2. (a) The chemical structure of poly(styrene)-*b*-poly(1,4-butadiene) (SB). (b,c) TEM images reveal the particle (bcc) and cylindrical (hex) morphologies of samples SB-20 and SB-25, respectively. Scale bars represent 0.2 μm. (d) DMTA data (shifted for clarity by indicated values) showing the ODTs for three samples, indicated by solid black arrows. An order-order transition is evident in blend-0.5, and is indicated by the dashed arrow. These isochronal experiments (1 rad/s) were performed in the linear regime (≤ 3 % strain) at heating and cooling rates of 1 ºC/min.

Heating and cooling sample SB-20 at 1 ºC/min through T_{ODT} while recording G'(1 rad/s) reveals hysteresis in the first-order transition between the bcc and dis phases, likely a consequence

of chain exchange mediated nucleation and growth of the particle-based cubic phase. Conversely, the hex ↔ dis transition with SB-25 exhibits virtually no hysteresis, which we associate with a diffusion-free transition mechanism involving fusion of fluctuating particles during cooling and fission of cylinders upon heating through T_{ODT}. This hypothesis regarding different phase transition mechanisms is supported by the observation that hex order fully develops in less than 2 minutes when sample SB-25 is rapidly cooled (ca. 100 ºC/min) from 230 ºC to 160 ºC, whereas ordering in SB-20 after quenching to 125 ºC from disorder takes several hours (Fig. 3).

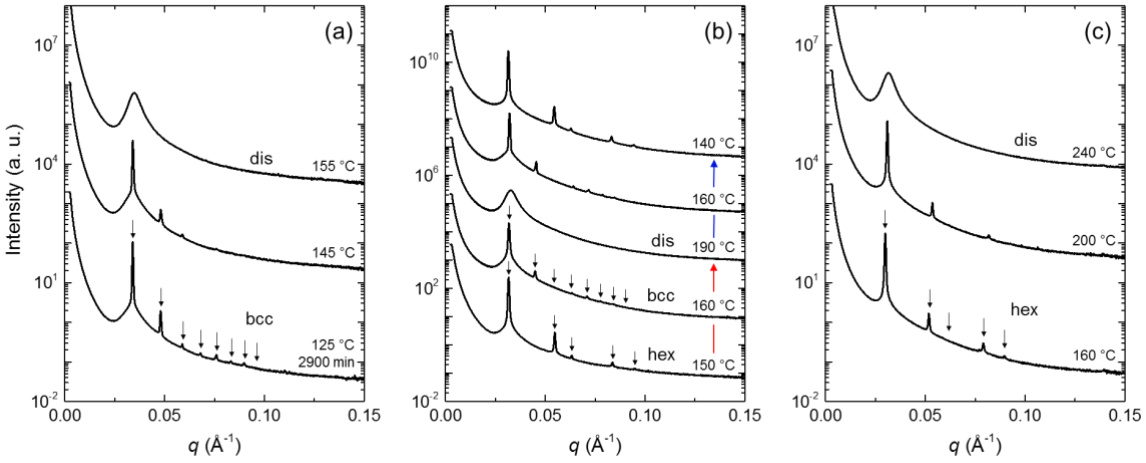

FIG. 3. Scattering profiles for samples SB-20 (a), blend-0.5 (b), and SB-25 (c). Black arrows indicate bcc ($(q/q^*)^2$ = 1, 2, 3, 4, 5, 6, 7, 8) or hex ($(q/q^*)^2$ = 1, 3, 4, 7, 9) reflections. Samples were held at each temperature for 2 minutes unless otherwise specified. In panel (b), the red and blue arrows indicate heating and cooling, respectively, at a rate of 100 ºC/min. Curves have been shifted vertically for clarity.

In order to establish the phase behavior of the SB system at intermediate compositions between the bcc and hex phases, we blended SB-20 and SB-25 at various ratios and characterized the states of order and disorder by monitoring G' and performing SAXS experiments as a function of temperature. Blending asymmetric diblock copolymers can lead to the formation of a variety of Frank-Kasper phases as recently demonstrated by SCFT calculations [39] and experimentally by Schulze *et al.* [18]. However, the relatively small differences in the degrees of polymerization ($\gamma = N_{SB\text{-}25}/N_{SB\text{-}20}$ = 1.18) and compositions associated with SB-20 and SB-25 places these blends below the SCFT predicted thresholds for inducing such structures, as shown in Fig. 4a.

Additionally, regions of phase coexistence in the blend diagram (mandated for binary mixtures by the Gibbs phase rule) are anticipated to be very narrow; $\Delta T_{\text{bcc-hex}}$ and ΔT_{ODT} are both predicted to be less than 1 ºC over the range of χN covered by the experiments (see Fig. S7 [26]). Hence, this blending technique should provide an efficient way to precisely locate ODT and order-order transition (OOT) phase boundaries as a function of f_{A} and temperature, enabling us to establish whether the σ phase exists at compositions between the bcc and hex morphologies. Five blends, denoted blend-ϕ, where ϕ represents the volume fraction of SB-20, were prepared by dissolution of measured amounts of each component in benzene followed by freeze-drying.

Fig. 2 shows G'(1 rad/s) obtained while heating and cooling blend-0.5 between 140 ºC and 185 ºC at 1 ºC/min. A reversible OOT is evidenced by the sharp increase in the elastic modulus at 160 ºC during heating and recovery of the lower-temperature elasticity at about 150 ºC while cooling. SAXS results shown in Fig. 3b reveal hex and bcc symmetry at the lower and higher temperatures, respectively. Hysteresis associated with the ODT and OOT during heating and cooling is consistent with the first-order nature of these phase transitions. Fig. 4b illustrates the phase diagram for all five binary blends as well as the neat precursors, where $\langle N \rangle = \phi N_{\text{SB-20}} + (1 - \phi) N_{\text{SB-25}}$ and $\chi = \alpha T^{-1} - \beta$ has been calculated using published T_{ODT} values for compositionally symmetric ($f_{\text{PB}} = ½$) SB based on the symmetric ROL theory (see Supplemental Material [26]). These results conclusively demonstrate that the SB system is devoid of the σ phase in the vicinity of the bcc-hex phase boundary for $f_{\text{PB}} < ½$ and near $(\chi N)_{\text{ODT}}$, in sharp contrast with the behavior of EL (Fig. 1b), notwithstanding identical conformational asymmetries of $\varepsilon = 1.7$. We believe the structures reported in Fig. 4b are equilibrium states based upon the facile transitions observed in both DMTA and SAXS results in Figs. 2d and 3, respectively. Moreover, formation of complex phases, such as the σ phase, is typically accompanied by the emergence of one or multiple small peaks in the vicinity of q^* from SAXS measurements, which we did not observe over the timescales of these experiments. The issues of dynamics and chain kinetics in the SB system in the context of complex phase formation is the subject of a future study.

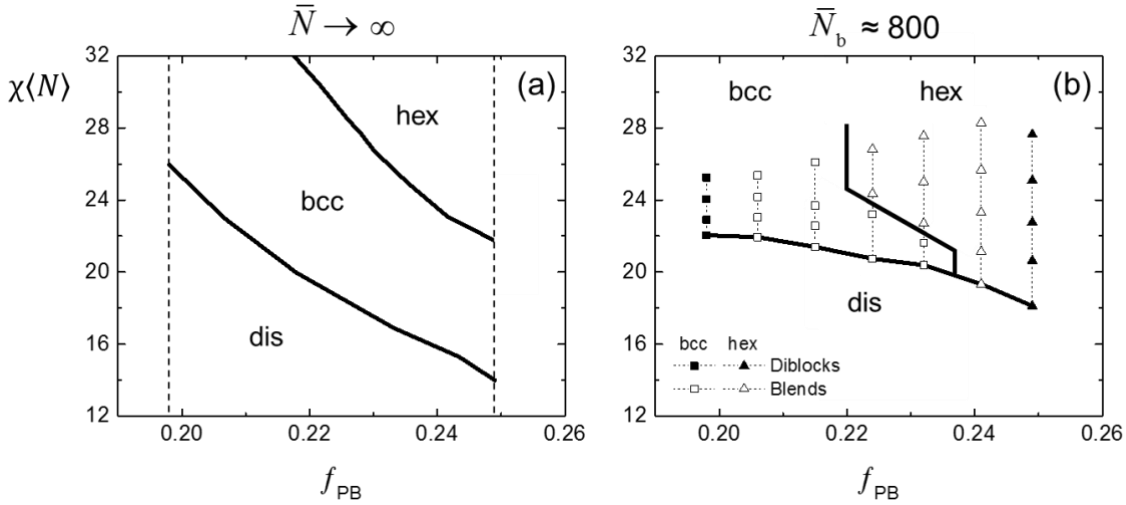

FIG 4. Mean-field (a) and experimental (b) phase diagrams obtained from binary blends of SB-20 and SB-25. Dashed lines in (a) represent the compositions of the pure diblock copolymers. Very narrow two-phase windows, represented by the solid curves in panel (a), have been omitted for simplicity but are shown in Fig. S7 [26].

A finite $\bar{N}$ has a predictable effect on the phase behavior of symmetric diblock copolymers in the vicinity of the lam ↔ dis transition [24, 25, 45]. Much less is known about the consequences of molecular weight in the asymmetric composition limit. Comparison of Figs. 1 and 4 demonstrates that increasing $\bar{N}_b$ from about 80 to 800 dramatically alters the phase behavior, where the SB system is remarkably consistent with the mean-field predictions. (We interpret termination of the experimental bcc-hex phase boundary at the ODT as a result of composition fluctuations, which truncate the bottom of the mean-field phase diagram.) Quantitative differences between Figs. 4a and 4b, most notably $(\chi N)_{ODT}$ at the lowest values of f_{PB}, are within the uncertainties associated with our estimate of $\chi(T)$ based on independent data obtained from f_{PB} = ½ diblock copolymers; a modest composition dependence could account for the differences. The most striking feature is extinction of the σ phase. This implies that the universal features captured by SCFT in the limit $\bar{N} \to \infty$ become distorted when $\bar{N}_b < \bar{N}_x$, presumably due to amplification of the effects of conformational asymmetry when chains are forced to fill space with a substantial self-concentration. We note that chain length dispersity may also play an important role, especially in the EL system, which has a broader distribution of particle core (PLA) chain lengths centered on a much smaller average degree of polymerization than that associated with SB (see

Supplemental Material [26]). Additionally, the findings of this study hinge on the assumption that the differences in chemical details of the SB and EL systems do not contribute significantly to the difference in observed phase behavior (aside from segregation strength effects).

The conclusions of this work are consistent with the recent explosion in the number of reports describing Frank-Kasper phases in surfactant systems [5–7], which conform to the $\bar{N}_b < \bar{N}_x$ limit. These findings also explain why tetrahedral packing has not been encountered in diblock copolymers until recently. The most studied system, SI (and SIS triblock copolymers), has $\bar{N}$ comparable to SB near the ODT and a smaller $\varepsilon = 1.25$ [28]. Moreover, most detailed investigations have focused on PS spheres, which place the smaller statistical segment length in the core of the domains, a configuration that does not support the formation of Frank-Kasper phases as shown by SCFT [17]. The results of this study place an empirical bound on the predictions of self-consistent field theory and motivate additional theoretical work in the $\bar{N}_b < \bar{N}_x$ limit.

Support for this work was provided by the National Science Foundation under Grants DMR-1104368 and DMR-1725272. This work is based upon work supported by the National Science Foundation Graduate Research Fellowship under Grant No. 00039202. SAXS experiments were conducted at the Advanced Photon Source (APS), Sector 5 (DuPont-Northwestern-Dow Collaborative Access Team, DND-CAT). DND-CAT is supported by E.I. DuPont de Nemours & Co., The Dow Chemical Company, and Northwestern University. Use of the APS, an Office of Science User Facility operated for the U.S. Department of Energy (DOE) Office of Science by Argonne National Laboratory, was supported by the U.S. DOE under Contract No. DE-AC02-06CH11357. Data were collected using an instrument funded by the National Science Foundation under Grant No. 0960140. Additionally, experiments were carried out in the Characterization Facility at the University of Minnesota, which receives partial support from the NSF through the MRSEC program. Computational resources to perform SCFT calculations are provided by the Minnesota Supercomputing Institute.

References:

[1] X. Zeng, G. Ungar, Y. Liu, and V. Percec, Nature **428**, 157 (2004).

[2] M. Huang, K. Yue, J. Wang, C.-H. Hsu, L. Wang, and S. Z. D. Cheng, Sci. China Chem. **59**, (2016).

[3] X. Feng, R. Zhang, Y. Li, Y. L. Hong, D. Guo, K. Lang, K. Y. Wu, M. Huang, J. Mao, C. Wesdemiotis, Y. Nishiyama, W. Zhang, T. Miyoshi, T. Li, and S. Z. D. Cheng, ACS Cent. Sci. **3**, 860 (2017).

[4] G. Ungar, V. Percec, X. Zeng, and P. Leowanawat, Isr. J. Chem. **51**, 1206 (2011).

[5] S. A. Kim, K.-J. Jeong, A. Yethiraj, and M. K. Mahanthappa, Proc. Natl. Acad. Sci. **114**, 4072 (2017).

[6] C. M. Baez-Cotto and M. K. Mahanthappa, ACS Nano **12**, 3226 (2018).

[7] A. Jayaraman and M. K. Mahanthappa, Langmuir **34**, 2290 (2018).

[8] S. Lee, M. J. Bluemle, and F. S. Bates, Science. **330**, (2010).

[9] T. M. Gillard, S. Lee, and F. S. Bates, Proc. Natl. Acad. Sci. **113**, 5167 (2016).

[10] K. Kim, M. W. Schulze, A. Arora, R. M. Lewis, III, M. A. Hillmyer, K. D. Dorfman, and F. S. Bates, Science. **356**, 520 (2017).

[11] F. C. Frank and J. S. Kasper, Acta Crystallogr. **11**, 184 (1958).

[12] F. C. Frank and J. S. Kasper, Acta Crystallogr. **12**, 483 (1959).

[13] A. C. Lawson, C. E. Olsen, J. W. Richardson, M. H. Mueller, and G. H. Lander, Acta Crystallogr. Sect. B **44**, 89 (1988).

[14] J. Hafner and D. Hobbs, Phys. Rev. B - Condens. Matter Mater. Phys. **68**, 14408 (2003).

[15] M. H. F. Sluiter and A. Pasturel, Phys. Rev. B - Condens. Matter Mater. Phys. **80**, 134122 (2009).

[16] S. Lee, C. Leighton, and F. S. Bates, Proc. Natl. Acad. Sci. U. S. A. **111**, 17723 (2014).

[17] N. Xie, W. Li, F. Qiu, and A. Shi, ACS Macro Lett. **3**, 906 (2014).

[18] M. W. Schulze, R. M. Lewis, III, J. H. Lettow, R. J. Hickey, T. M. Gillard, M. A. Hillmyer, and F. S. Bates, Phys. Rev. Lett. **118**, 207801 (2017).

[19] H. Tao, T. P. Lodge, and E. D. Von Meerwall, Macromolecules 33, 1747 (2000).

[20] G. C. Berry and T. Fox, Adv. Polym. Sci. **5**, 261 (1968).

[21] L. J. Fetters, D. J. Lohse, D. Richter, T. A. Witten, and A. Zirkel, Macromolecules **27**, 4639 (1994).

[22] G. Ronca, J. Chem. Phys. **79**, 1031 (1983).

[23] T. A. Kavassalis and J. Noolandi, Phys. Rev. Lett. **59**, 2674 (1987).

[24] P. Medapuram, J. Glaser, and D. C. Morse, Macromolecules **48**, 819 (2015).

[25] J. Glaser, P. Medapuram, T. M. Beardsley, M. W. Matsen, and D. C. Morse, Phys. Rev. Lett. **113**, 1 (2014).

[26] See Supplemental Material, which includes Refs. [25-35], information regarding sample synthesis, molecular and physical characterization techniques, interaction parameter calculation, and mean-field theory details.

[27] M. A. Hillmyer and F. S. Bates, Macromolecules **29**, 6994 (1996).

[28] A. K. Khandpur, S. Förster, F. S. Bates, I. W. Hamley, A. J. Ryan, W. Bras, K. Almdal, and K. Mortensen, Macromolecules **28**, 8796 (1995).

[29] H. L. Wagner, J. Phys. Chem. Ref. Data **14**, 1101 (1985).

[30] M. W. Matsen and M. Schick, Phys. Rev. Lett. **72**, 2660 (1994).

[31] M. W. Matsen, J. Phys. Condens. Matter **14**, R21 (2002).

[32] A. Arora, J. Qin, D. C. Morse, K. T. Delaney, G. H. Fredrickson, F. S. Bates, and K. D. Dorfman, Macromolecules **49**, 4675 (2016).
[33] C. M. Papadakis, W. Brown, R. M. Johnsen, D. Posselt, and K. Almdal, J. Chem. Phys. **104**, 1611 (1996).
[34] M. D. Gehlsen and F. S. Bates, Macromolecules **27**, 3611 (1994).
[35] P. J. Flory, J. Am. Chem. Soc. **62**, 1561 (1940).
[36] N. A. Lynd and M. A. Hillmyer, Macromolecules **38**, 8803 (2005).
[37] K. S. Anderson and M. A. Hillmyer, Macromolecules **37**, 1857 (2004).
[38] J. Qin and D. C. Morse, Phys. Rev. Lett. **108**, 11 (2012).
[39] T. Ghasimakbari and D. C. Morse, Macromolecules **51**, 2335 (2018).
[40] M. W. Matsen and F. S. Bates, J. Polym. Sci. Part B Polym. Phys. **35**, 945 (1997).
[41] M. Liu, Y. Qiang, W. Li, F. Qiu, and A.-C. Shi, ACS Macro Lett. **5**, 1167 (2016).
[42] C. D. Han, N. Y. Vaidya, D. Kim, G. Shin, D. Yamaguchi, and T. Hashimoto, Macromolecules **33**, 3767 (2000).
[43] S. Foerster, A. Khandpur, J. Zhao, F. S. Bates, I. W. Hamley, A. J. Ryan, and W. Bras. Macromolecules **27**, 6922 (1994).
[44] M. Schwab and B. Stühn, Colloid Polym. Sci. **275**, 341 (1997).
[45] T. Jun, Y. Lee, S. Jo, C. Y. Ryu, and D. Y. Ryu, Macromolecules **51**, 282 (2017).